

A Fidelity Study of the Superconducting Phase Diagram in the 2D Single-band Hubbard Model

C. J. Jia,^{1,2} B. Moritz,^{1,3} C.-C. Chen,^{1,4} B. Sriram Shastry,⁵ and T. P. Devereaux^{1,6}

¹*Stanford Institute for Materials and Energy Sciences,
SLAC National Accelerator Laboratory, 2575 Sand Hill Road, Menlo Park, CA 94025.*

²*Departments of Applied Physics, Stanford University, CA 94305.*

³*Department of Physics and Astrophysics, University of North Dakota, Grand Forks, ND 58202, USA*

⁴*Departments of Physics, Stanford University, CA 94305.*

⁵*Department of Physics, University of California, Santa Cruz, CA 95064.*

⁶*Geballe Laboratory for Advanced Materials, Stanford University, CA 94305.*

(Dated: August 2, 2022)

Extensive numerical studies have demonstrated that the two-dimensional single-band Hubbard model contains much of the key physics in cuprate high temperature superconductors. However, there is no definitive proof that the Hubbard model truly possesses a superconducting ground state, and if it does, how it depends on model parameters. To answer these longstanding questions, we study an extension of the Hubbard model including an infinite-range d -wave pair field term which precipitates a superconducting state in the d -wave channel. Using cluster exact diagonalization, we study the evolution of eigenstates as a function of the strength of the pairing term. This is achieved by monitoring the fidelity metric of the ground state and the ratio between the two largest eigenvalues of the d -wave pair density matrix. The calculations show antiferromagnetic and a checkerboard charge density wave ground states on the underdoped and overdoped sides of the phase diagram, respectively, with the strength controlled by the Coulomb repulsion U and the next-nearest-neighbor hopping t' , respectively; these two orders bracket a d -wave superconducting state near 25% hole-doping. The results also demonstrate that t' plays an important role in the formation of d -wave superconductivity.

PACS numbers: 71.10.Fd, 74.25.Dw, 03.65.Aa, 74.72.-h

I. INTRODUCTION

Originally proposed for the study of transition metals, the Hubbard model¹ continues to be one of the simplest, and yet complex models, used to describe strongly correlated systems and possibly the cuprate high temperature superconductors^{2,3}. However, despite over 40 years of intensive numerical and analytical studies and over 20 years devoted to the connection with superconductivity in cuprates, the repulsive Hubbard model in two dimensions has not been proven to possess a unique superconducting (SC) ground state in any parameter space apart from asymptotically small coupling with a vanishingly small transition temperature^{4,5}. Promisingly, recent dynamical cluster approximation calculations suggest the presence of finite temperature d -wave superconductivity near half-filling^{6,7}.

Empirically, in terms of the underlying non-interacting band structure, the SC transition temperature is larger in materials possessing bonding Fermi surfaces far from $(\pi, 0)$ with only a small portion nesting the antiferromagnetic reciprocal lattice vector $Q = (\pi, \pi)$ ^{8,9}. This degree of Fermi surface bending is related to the strength of the hopping parameter along the diagonals of the unit cell - the next-nearest-neighbor hopping $t' (< 0)$ - in the single-band model for the electronic dispersion. Pavarini *et al.* give reasons why a large t' (the absolute value) might favor superconductivity due to the minimization of the hybridization of Cu orbitals with apical oxygen

orbitals⁸. However, most numerical studies of superconductivity in the single-band Hubbard model do not show a strong dependence on t' - in fact most studies of the t - J and the Hubbard model indicate that t' hurts superconductivity¹⁰⁻¹⁵.

In addition, the phase diagram of several materials in the cuprate family has displayed several tendencies to show charge ordering in doped systems, forming either static stripes as revealed in neutron scattering studies of LaBaCuO and related compounds^{16,17}, or local checkerboard-type order on the level of a few lattice spacings as revealed by scanning tunneling spectroscopy (STS) on superconducting $\text{Bi}_2\text{Sr}_2\text{CaCu}_2\text{O}_{8+x}$ and $\text{Bi}_2\text{Sr}_2\text{CuO}_{6+x}$ ¹⁸⁻²³. Moreover, recent angle-resolved photoemission (ARPES)²⁴ on nearly optimally doped $\text{Bi}_2\text{Sr}_2\text{CuO}_{6+x}$ have revealed a density-wave type of order emerging below temperatures T^* above T_c . This propensity for charge ordering in doped systems gives an indication that a density-wave type of instability may also lie in close proximity as a competing phase to the dominant superconducting order parameter, and suggests that higher superconducting transition temperatures might be obtained as a result of controlling the emergence of the density-wave phase. After such a long period of study, it remains an open question whether this model has enough physics to capture the essence of the ground state phases in the cuprates as a function of doping or other material parameters.

Our aim is to investigate the conjecture that the Hub-

bard model could possess a d -wave SC ground state, and other postulated phases that either compete or coexist with d -wave superconductivity. For this, we study an extension of the Hubbard model, including an infinite-range d -wave pair field term of strength λ which precipitates SC in the d -wave channel. The method of adding a pair field term to a standard low-energy Hamiltonian was introduced earlier by Rigol, Shastry and Haas (RSH) for the study of superconductivity in the t - J model^{25,26}. Thus, our Hamiltonian guarantees a d -wave SC ground state for sufficiently strong λ . By gradually decreasing λ , one expects a quantum phase transition (QPT), or in a finite size cluster a quantum critical crossover (QCC), provided the Hubbard model does not favor a d -wave SC ground state. Otherwise, if no QPT or QCC is observed, we infer that the bare Hubbard model possesses a d -wave SC ground state. We establish a criterion for the existence of the QCC by monitoring the fidelity metric g [Ref. 27–30] as a function of λ . We perform the calculations for the 2D single-band Hubbard model near half-filling for different values of the Coulomb repulsion U and the next-nearest-neighbor hopping t' . We also study physical properties of various competing orders, including antiferromagnetism and charge density wave (CDW) order, to understand the phase transition between d -wave SC and other phases as λ gradually decreases. For this purpose and to identify the nature of various other phases, we study the density matrix eigenvalues and their ratios, as discussed below in Eq. (5)-(7).

The rest of the paper is organized as follows. In section II we present our calculational methodology and justify the use of the fidelity metric to monitor the change of orders in ground states. In section III we present and discuss our results from finite size cluster exact diagonalization (ED) studies of the single-band Hubbard model for various cluster sizes, hole-dopings and other model parameters. We find that the phase diagram contains antiferromagnetism and CDW ground states on the underdoped and overdoped sides of the phase diagram, respectively, bracketing a d -wave SC state near 25% hole-doping. Moreover, we find that the antiferromagnetic order is mainly controlled by U , while the CDW order is determined by t' . Finally, we offer a summary of our results and interpretations in section IV.

II. CALCULATION METHODOLOGY

A. Model Hamiltonian

The single-band Hubbard model is described by the Hamiltonian

$$H_{\text{Hubbard}} = - \sum_{i,j,\sigma} t_{ij} c_{i\sigma}^\dagger c_{j\sigma} + \sum_i U n_{i\uparrow} n_{i\downarrow}, \quad (1)$$

where $c_{i\sigma}^\dagger$ ($c_{i\sigma}$) creates (annihilates) an electron with spin σ on lattice site i , t_{ij} are overlaps or “hopping” inte-

grals restricted to the nearest-neighbor and next-nearest-neighbor, denoted as $t(>0)$ and $t'(<0)$, U is the on-site Coulomb repulsion, and $n_{i\sigma} = c_{i\sigma}^\dagger c_{i\sigma}$ is the number operator.

To ensure a d -wave SC ground state, we introduce a d -wave pair field term of the BCS type with a d -wave order parameter³¹:

$$H_{d\text{-wave}} = - \frac{\lambda}{N} \sum_{i,j} D_i^\dagger D_j, \quad (2)$$

where $D_i = \Delta_{i,i+\hat{x}} - \Delta_{i,i+\hat{y}}$, $\Delta_{ij} = c_{i\uparrow} c_{j\downarrow} + c_{j\uparrow} c_{i\downarrow}$, λ is the strength of this d -wave BCS attraction, and N is the total number of the lattice sites. We will assume that λ changes between 0 and $O(1)$, in units of t .

RSH have shown that for the t - J model plus a d -wave pair field term with strength λ , a SC ground state is present at some sufficiently large λ in small clusters^{25,26}. Similar to this model, we assume our Hamiltonian possesses a d -wave SC ground state when λ is sufficiently large in any finite size cluster, without loss of generality. Thus, we view λ as a “continuous switch”, to study the Hubbard model containing a d -wave SC ground state: when λ is large or “on”, the d -wave BCS term is dominant and the Hamiltonian exhibits a d -wave SC ground state; as λ approaches zero or the “off” state, the Hamiltonian reduces to that of the bare Hubbard model, thus revealing the properties of its ground state. This is completely analogous to the study of ground state magnetism by slowly switching off an applied magnetic field. In summary, we begin with a large λ , utilize the assumed d -wave SC ground state as a starting point, and gradually decrease λ . If a QCC does not occur, as indicated by the behavior of the fidelity metric defined in the following section, it illustrates that the Hubbard model ground state has the same characteristic as the ground state at large λ – a d -wave SC state; if a QCC occurs, it demonstrates a change in the ground state phase, indicating that the Hubbard model does not possess a d -wave SC ground state. The nature of the non-SC state is then determined from a study of the density matrix, as elaborated below.

B. Fidelity metric

The main point of this work, capturing a possible QCC between the d -wave SC state and other phases, can be accomplished by calculating a quantity known as fidelity. Fidelity first was used widely in quantum information to provide the criterion for distinguishing between quantum states^{32,33} and now has been utilized increasingly in general physics for investigating classical as well as quantum critical behavior in various systems^{27–30,34–38}. The work with fidelity on fermionic models and spin models recently has received increased attention related to QPT and is powerful enough for non-standard QPT like topological phase transitions^{30,37} where no direct examination can be made of an order parameter.

Given a Hamiltonian of the form $H(\lambda) = H_0 + \lambda H_1$, the square modulus of the overlap between the perturbed and unperturbed ground state $F(\lambda, \delta\lambda) = \langle \Phi_0(\lambda) | \Phi_0(\lambda + \delta\lambda) \rangle$ defines the fidelity.

In time-independent perturbation theory, $|\Phi_0(\lambda + \delta\lambda)\rangle$ can be expanded in the normalized eigenstates at λ : $|\Phi_\alpha(\lambda)\rangle$ ($\alpha = 0, 1, 2, \dots$); and to second order in $\delta\lambda$ the term proportional to the unperturbed ground state is

$$\langle \Phi_0(\lambda) | \Phi_0(\lambda + \delta\lambda) \rangle = 1 - \frac{\delta\lambda^2}{2} \sum_{\alpha \neq 0} \frac{|\langle \Phi_\alpha(\lambda) | H_1 | \Phi_0(\lambda) \rangle|^2}{[E_0(\lambda) - E_\alpha(\lambda)]^2} \quad (3)$$

The fidelity has been shown to be an extensive quantity in other Hamiltonians similar to our model^{28,35}. So following RSH, we introduce an intensive quantity, the fidelity metric²⁷⁻³⁰ defined as $g(\lambda, \delta\lambda) = (2/N)(1 - F(\lambda, \delta\lambda))/\delta\lambda^2$ (equivalent to the fidelity susceptibility defined in other contexts^{35,38}), whose limit is well defined as $\delta\lambda \rightarrow 0$

$$\lim_{\delta\lambda \rightarrow 0} g(\lambda, \delta\lambda) = \frac{1}{N} \sum_{\alpha \neq 0} \frac{|\langle \Phi_\alpha(\lambda) | H_1 | \Phi_0(\lambda) \rangle|^2}{[E_0(\lambda) - E_\alpha(\lambda)]^2}. \quad (4)$$

The fidelity metric evolves smoothly away from critical points where it diverges and perturbation theory fails. By approaching a quantum critical point from either direction, the fidelity metric can be a powerful tool to signal a QPT/QCC by a dramatic increase (or drop)²⁷ at the critical point. We find the fidelity metric is independent of the value of $\delta\lambda$ when λ is between $O(10^{-5})$ and $O(10^{-3})$; however the fidelity metric behaves substantially different when $\delta\lambda$ is smaller and larger, coming from numerical errors and lack of accuracy, respectively. Thus in what follows we use $\delta\lambda = 3 \times 10^{-4}$ to balance these two concerns well at the same time.

C. d -wave pair density matrix

While the fidelity metric captures the existence of a QPT/QCC, we also would like to investigate quantities directly related to the order parameter. The d -wave pair density matrix^{25,39,40} can be defined as

$$P_{ij}^{d-wave} = \langle \Phi_0 | D_i^\dagger D_j | \Phi_0 \rangle \quad (5)$$

with the ratio between the largest and next largest eigenvalues given by $R_{d-wave} = \Lambda_1(P_{ij}^{d-wave})/\Lambda_2(P_{ij}^{d-wave})$. The study of the ratio R_{d-wave} was first suggested by RSH. To understand its significance, we note that based on the work of Penrose and Onsager⁴¹ particle condensation into some well defined ordered state leads to characteristic behavior in the corresponding density matrix: the largest eigenvalue scales to a finite value greater than $O(1)$ while the other eigenvalues $\sim O(1)$. Further Yang³⁹ showed that the largest eigenvalue actually scales linearly with the total number of particles. Thus, $R_{d-wave} \sim \Psi^2 N + \Phi$, where Ψ is the order parameter and Φ is sub-linear in the system size. In other words,

the ratio R_{d-wave} , having an intrinsic correlation to this d -wave SC order parameter, can be used directly to investigate d -wave SC order. A similar analysis follows for other (non-SC) orderings.

D. Other quantities of interest

Besides superconductivity, both charge and spin orders have been reported in high T_c SC materials, with the undoped parent compounds known to be antiferromagnetic Mott insulators. Moreover, the 2D Hubbard model for sufficiently strong Coulomb repulsion U possesses a well known strong antiferromagnetic order at half-filling. Thus, we study both charge and spin orders by calculating the charge and spin density matrices:

$$P_{ij}^{spin} = \langle \Phi_0 | \sigma_{zi} \sigma_{zj} | \Phi_0 \rangle, \quad (6)$$

$$P_{ij}^{charge} = \langle \Phi_0 | \rho_i \rho_j | \Phi_0 \rangle, \quad (7)$$

where $\sigma_{zi} = c_{i\uparrow}^\dagger c_{i\uparrow} - c_{i\downarrow}^\dagger c_{i\downarrow}$ and $\rho_i = c_{i\uparrow}^\dagger c_{i\uparrow} + c_{i\downarrow}^\dagger c_{i\downarrow}$. We investigate both $R_{spin} = \Lambda_1(P_{ij}^{spin})/\Lambda_2(P_{ij}^{spin})$ and $R_{charge} = \Lambda_1(P_{ij}^{charge})/\Lambda_2(P_{ij}^{charge})$, as we do for the d -wave pair density matrix, as well as specific matrix elements associated with the charge and spin correlation functions. This approach can capture the strength of possible competing charge and spin orders.

III. RESULTS

Before describing our numerics, we clarify our viewpoint. Based on the experience in RSH, we look at the fidelity metric g , together with the ratio R of the largest to next largest eigenvalue of the density matrix - with suitable symmetry. It is a combined look at these variables g and R as functions of λ that enable us to draw conclusions about the nature of ordering. We note that a peak in g usually signifies a crossover between two phases, and a jump in g signifies a level crossing. We denote by λ^* the location of the peak in $g(\lambda)$, and it is seen below to play an important role in the analysis. The ratio R has a magnitude ~ 1 , when the symmetry of the order parameter is incompatible with the ground state. It is large (3-10 in the t - J model studied in RSH) when the symmetry is compatible, for small systems. In the limit of large systems, which is currently unattainable, it is not possible to assert that a quantum critical point exists, but looking at g and R together gives us a reasonable picture of the evolution of the ground state.

We perform the calculations with the ED technique in a finite size cluster using the Parallel ARnoldi PACKage (PARPACK)⁴². The size of the Hilbert space grows exponentially with increasing cluster size. Considering symmetries, including the total number of electrons and total momentum, and fixing ourselves in the space with

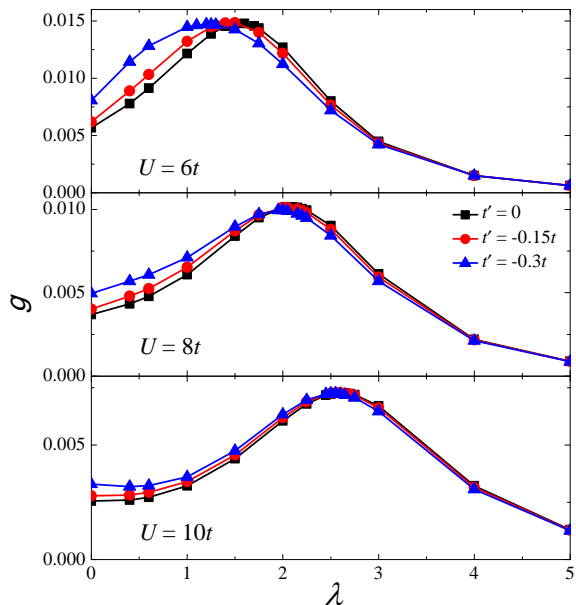


FIG. 1: The fidelity metric g as a function of d -wave pair field strength λ at half-filling. Coulomb $U(6t, 8t, 10t)$ and $t'(0, -0.15t, -0.3t)$ are indicated. The small magnitude of g indicates the incompatibility of d -wave order at half-filling.

total spin $S_z = 0$, the size of the Hamiltonian is diminished to $\sim 10^7$ so that ED could be accomplished using PARPACK in a reasonable time. We perform the calculations for the 16B Betts cluster⁴³. Due to computational time considerations, we don't perform any calculations for clusters larger than 16. The 16B Betts cluster provides access to momentum $(\pi/2, \pi/2)$, where the d -wave SC gap starts to open and many low energy excitations exist. Thus, we present calculations using the 16B Betts cluster in the following sections.

A. Antiferromagnetic Order at Half-filling

The fidelity metric g at half-filling for various values of U and t' is shown in Fig. 1. g approaches a small value as $\lambda \rightarrow 0$, and $g \rightarrow 0$ as λ increases beyond the peak value. These two regions correspond to two different phases: the d -wave SC state at large λ , and the competing state at small λ . λ^* is larger than 1, implying that this competing state exhibits strong order which is even stronger as U increases, since it requires a large d -wave λ to conquer the competing phase.

To obtain a full picture, we also calculate both $R_{d\text{-wave}}$ and R_{spin} as functions of λ with the results shown in Fig. 2. First, $R_{d\text{-wave}}$ reaches 1 as $\lambda \rightarrow 0$, which confirms the incompatibility of d -wave SC order in the Hubbard model at half-filling. Second, the large value of R_{spin} at $\lambda \rightarrow 0$ is consistent with the well known fact that the 2D Hubbard model at half-filling exhibits strong antiferromagnetic order. The values of R_{spin} at $\lambda \rightarrow 0$ increases for increasing U , demonstrating stronger antiferromag-

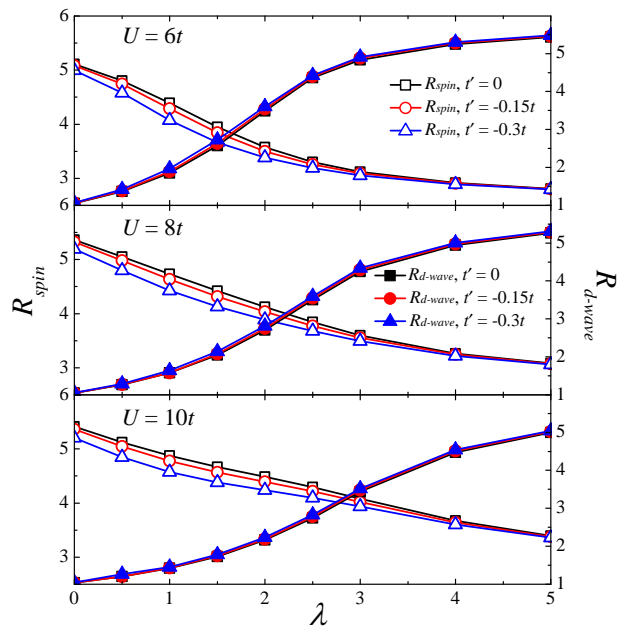


FIG. 2: The ratio of the largest to second largest eigenvalue of the d -wave pair density matrix $R_{d\text{-wave}}$ and that of the spin density matrix R_{spin} as functions of d -wave pair field strength λ at half-filling. Coulomb $U(6t, 8t, 10t)$ and $t'(0, -0.15t, -0.3t)$ are indicated.

netic order for larger values of U . Further examining the spin correlation functions (not shown) reveals a (π, π) antiferromagnetic order. Third, with the increase in λ , R_{spin} decreases and $R_{d\text{-wave}}$ increases, with a crossover at a certain λ . The crossover of R_{spin} and $R_{d\text{-wave}}$ in Fig. 2 moves to higher λ at larger U , consistent with the fidelity metric g shown in Fig. 1. Based on these points, the fidelity g in Fig. 1 is now more clearly understandable. The small peak at λ between 1 to 2.5 for various parameters arises from forcing d -wave SC order by the applied SC term in Eq. (2), and is best viewed as a crossover, rather than a QPT. In a strict sense we are thus studying QCC rather than quantum critical points.

We next study the effects of t' . Figure 1 shows that the QCC moves to lower values as t' increases. Moreover, Fig. 2 demonstrates that t' enhances only slightly the d -wave SC order measured by $R_{d\text{-wave}}$ while substantially suppressing the antiferromagnetic order as reflected in R_{spin} . This indicates that while t' may hurt the antiferromagnetic order, it does not necessarily lead to an enhancement of superconductivity at 1/2 filling. These effects in R_{spin} and $R_{d\text{-wave}}$ do not depend critically on the value of U for this range of parameters.

B. Hole-doping near Half-filling

Figure 3 shows results at 12.5% hole-doping that follow a similar trend as half-filling: as $\lambda \rightarrow 0$, g approaches a small finite value; as λ increases, g increases to a max-

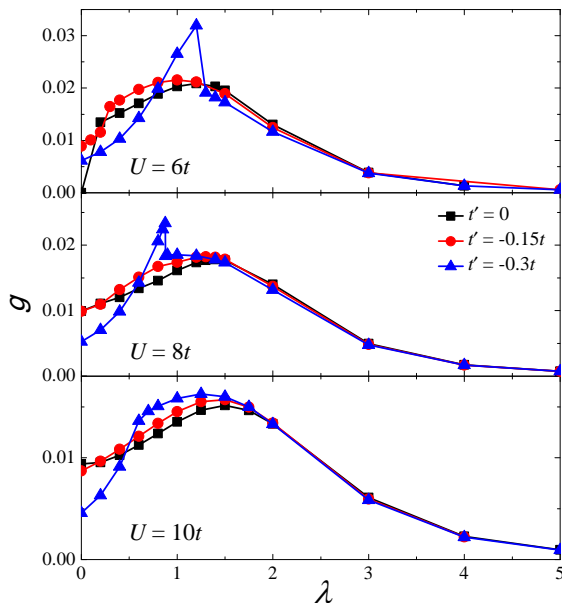


FIG. 3: The fidelity metric g as a function of d -wave pair field strength λ at 12.5% hole-doping. Coulomb $U(6t, 8t, 10t)$ and $t'(0, -0.15t, -0.3t)$ are indicated.

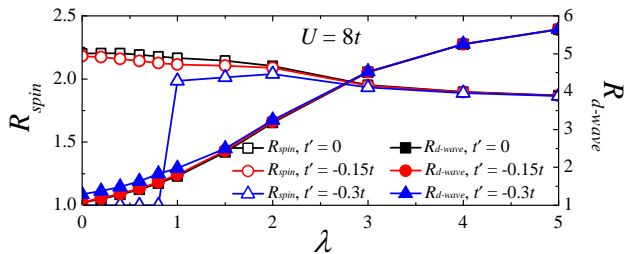


FIG. 4: The ratios of the largest to second largest eigenvalue of the d -wave pair density matrix R_{d-wave} and that of the spin density matrix R_{spin} as functions of d -wave pair field strength λ at 12.5% hole-doping. Coulomb $U = 8t$ and $t'(0, -0.15t, -0.3t)$ are indicated.

imum at some λ^* , and then decreases monotonically toward zero with additional increase in λ . This behavior indicates that the ground state of the Hubbard model is not a d -wave SC for this cluster size or parameter regime. The dependence of λ^* on U and t' is also similar to the results at half-filling, except for the discontinuities in g for $t' = -0.3t$ at $\lambda \sim 1.0$, stemming from an abrupt change in momentum sector of the ground state. This type of sudden change for these sets of parameters only occurs for this specific cluster, and should not occur in the thermodynamic limit. The trends in R_{d-wave} and R_{spin} as functions of λ at various values of U and t' are also similar to the results at half-filling shown in Fig. 2 – d -wave SC and spin order depend mainly on U and slightly on t' . As seen in Fig. 4, R_{spin} is larger than 1 as $\lambda \rightarrow 0$, however, smaller than at half-filling, implying the competing state is also antiferromagnetism but weaker than that at half-filling.

C. SC state at 25% hole-doping

Figure 5 shows the fidelity metric calculations at 25% hole-doping, with a log-linear scale employed to catch clearly the transition as $\lambda \rightarrow 0$. As seen in Fig. 5, λ^* moves close to zero or even negative values (see also Fig. 12) suggesting that the state remains in the same phase as λ is decreasing towards zero. In Fig. 6, the robust value of $R_{d-wave} \sim 10$ for $\lambda \sim 3$ is an indicator of d -wave SC order; R_{d-wave} persists to ~ 2 (but not as small as ~ 1) for $\lambda \sim 0$. This is evidence of the existence of d -wave SC order in the 2D single-band Hubbard model even without the d -wave pair field.

There is growing evidence that t' plays an important role on the critical temperature and other properties of SC materials^{8,10–15,44,45}. Our calculations support the statement that larger t' favors a d -wave SC state, demonstrated by the fidelity metric calculations shown in Fig. 5 where t' gives a rapid increase to the fidelity metric as λ goes to zero and yields $\lambda^* \rightarrow 0$ with increasing t' , and also by the d -wave pair density matrix calculations where R_{d-wave} (at $\lambda = 0$) has a larger value as t' increases. Notice there are sudden changes of g at $t' = 0, U = 6t, 8t$ or $10t$, only near $\lambda \rightarrow 0$, which do not originate from a change of momentum sector of the ground state as encountered in previous cases. These sudden changes are seen in Fig. 6 for R_{d-wave} as well, where R_{d-wave} jumps to 1 as $\lambda \rightarrow 0$. The eigenstates of the d -wave pair density matrix with the largest and second largest eigenvalues are degenerate, so the Cooper pairs distribute evenly into these two states⁴¹. In other words, d -wave SC order is incompatible in this system. This situation does not exist for non-zero t' , since t' breaks this degeneracy and forces the Cooper pairs to condense into the state with the largest eigenvalue.

D. Hole-doping far from Half-filling

In the overdoped region, fidelity metric calculations at 37.5% and 50% hole-doping display that λ^* is finite, indicating a ground state incompatibility with d -wave pairing as $\lambda \rightarrow 0$, and gives a λ^* that depends strongly on t' : at 37.5% hole-doping [Fig. 7], $\lambda^* \sim 0.25, 0.5$ and 0.75 at $t' = -0.3t, -0.15t$ and 0 ; at 50% hole-doping [Fig. 8], $\lambda^* \sim 0.25, 0.4$ and 0.6 at $t' = -0.3t, -0.15t$ and 0 . Since λ^* here is one order of magnitude smaller than the λ^* in the underdoped region, the competing state here is more easily suppressed by the d -wave pair field when compared to the strong antiferromagnetic order exhibited near half-filling.

Calculations of the charge density matrix and R_{charge} show that R_{charge} is always greater than 1 and does not change much as a function of λ , so tracking R_{charge} , by itself, might be insufficient to determine the change of charge order. We then focus on the charge correlation functions (CCFs) – the elements in the charge density matrix $P_{ij}^{charge} =$

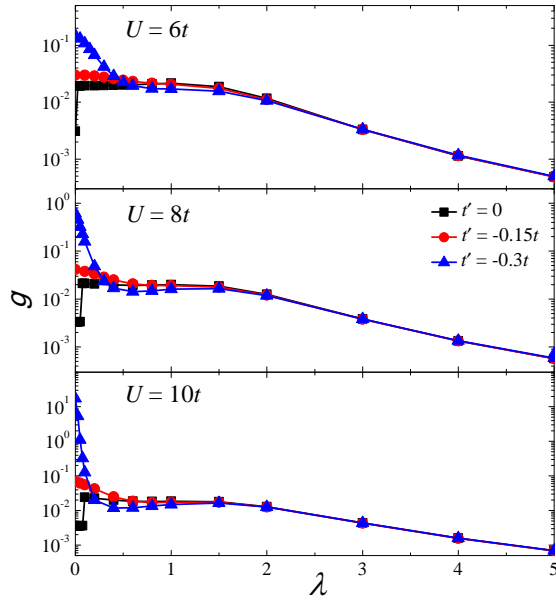


FIG. 5: The fidelity metric g as a function of d -wave pair field strength λ at 25% hole-doping. Coulomb $U(6t, 8t, 10t)$ and $t'(0, -0.15t, -0.3t)$ are indicated. A semi-log scale is employed to highlight the behaviors around $\lambda = 0$.

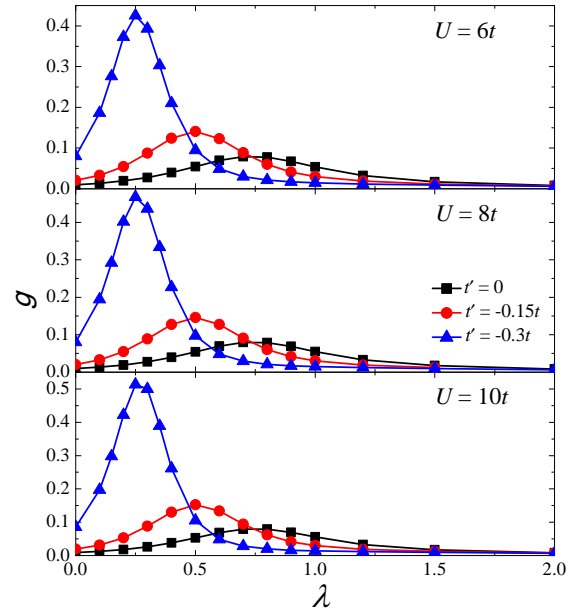


FIG. 7: The fidelity metric g as a function of d -wave pair field strength λ at 37.5% hole-doping. Coulomb $U(6t, 8t, 10t)$ and $t'(0, -0.15t, -0.3t)$ are indicated.

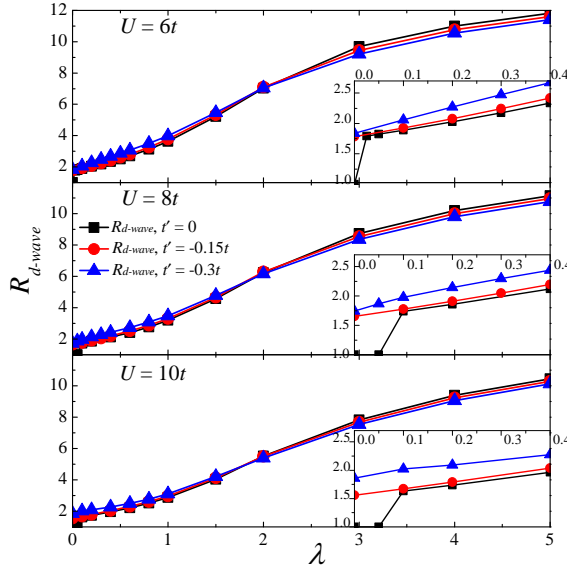


FIG. 6: The ratio of the largest to second largest eigenvalue of the d -wave pair density matrix R_{d-wave} as a function of d -wave pair field strength λ at 25% hole-doping. Coulomb $U(6t, 8t, 10t)$ and $t'(0, -0.15t, -0.3t)$ are indicated. The behaviors near $\lambda = 0$ are highlighted in the insets.

$\langle \Phi_0 | \rho_i \rho_j | \Phi_0 \rangle$, especially the normalized nearest-neighbor CCF (NN-CCF) $\langle \Phi_0 | \rho_r \rho_{r+\hat{x}} | \Phi_0 \rangle / \langle \Phi_0 | \rho_r \rho_r | \Phi_0 \rangle$, the 2NN-CCF $\langle \Phi_0 | \rho_r \rho_{r+\hat{x}+\hat{y}} | \Phi_0 \rangle / \langle \Phi_0 | \rho_r \rho_r | \Phi_0 \rangle$ and the 3NN-CCF $\langle \Phi_0 | \rho_r \rho_{r+2\hat{x}} | \Phi_0 \rangle / \langle \Phi_0 | \rho_r \rho_r | \Phi_0 \rangle$ - to observe how they evolve as functions of λ . Figures 9 through 11 show the normalized CCFs and R_{d-wave} at 37.5% doping for $U = 10t$, 50% doping for $U = 10t$ and 50% doping for

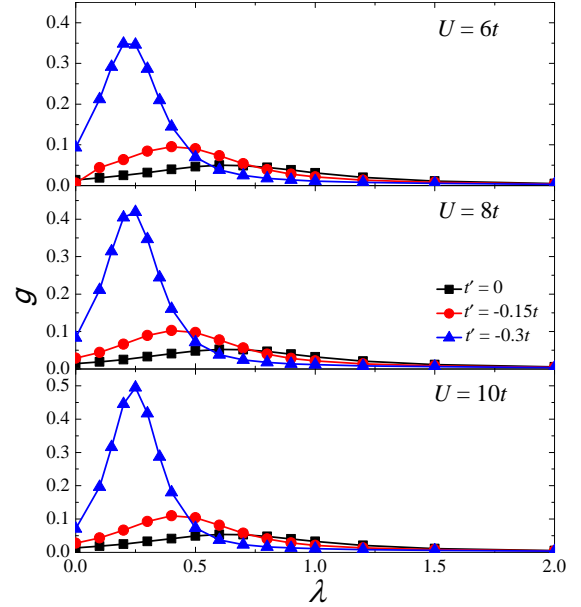


FIG. 8: The fidelity metric g as a function of d -wave pair field strength λ at 50% hole-doping. Coulomb $U(6t, 8t, 10t)$ and $t'(0, -0.15t, -0.3t)$ are indicated.

$U = 6t$. We observe a QCC between the d -wave SC state and some charge ordered state by the trends in the CCFs: the nearest-neighbor CCF increases while the other CCFs drop, as λ decreases. The variable R_{d-wave} increases with λ and is quite large. Specifically, at $\lambda = 0$, the diagonal CCF and the third-nearest-neighbor CCF dominate, while the nearest-neighbor CCF is small, showing a CDW state with checkerboard charge order. At

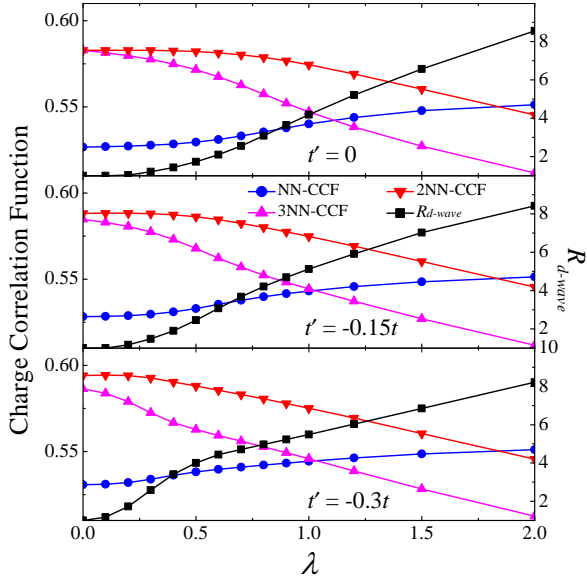


FIG. 9: The charge correlation functions (NN-CCF, 2NN-CCF and 3NN-CCF) and the ratio of the largest to second largest eigenvalue of the d -wave pair density matrix $R_{d\text{-wave}}$ as functions of d -wave pair field strength λ at 37.5% hole-doping. $U = 10t$ and $t'(0, -0.15t, -0.3t)$ are indicated.

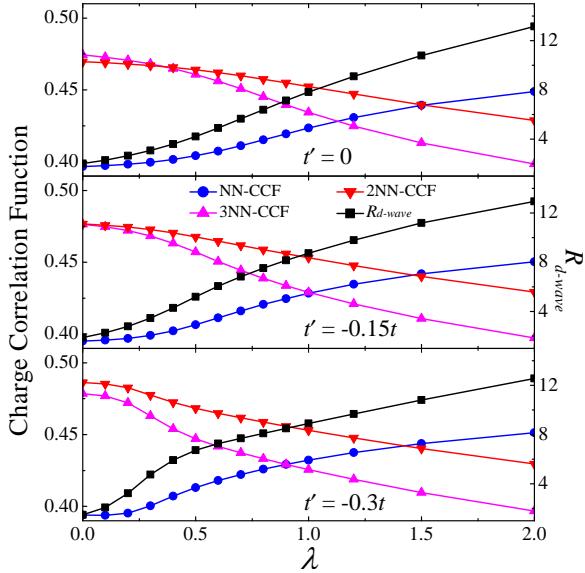


FIG. 10: The charge correlation functions (NN-CCF, 2NN-CCF and 3NN-CCF) and the ratio of the largest to second largest eigenvalue of the d -wave pair density matrix $R_{d\text{-wave}}$ as functions of d -wave pair field strength λ at 50% hole-doping. $U = 10t$ and $t'(0, -0.15t, -0.3t)$ are indicated.

large λ , this checkerboard CDW state is diminished, because the diagonal CCF and the third-nearest-neighbor CCF are suppressed and the nearest neighbor CCF is enhanced. This enhancement originates from the fact that Cooper pair formation favors nearest neighbor pairing. As λ gradually decreases, the phase transition from

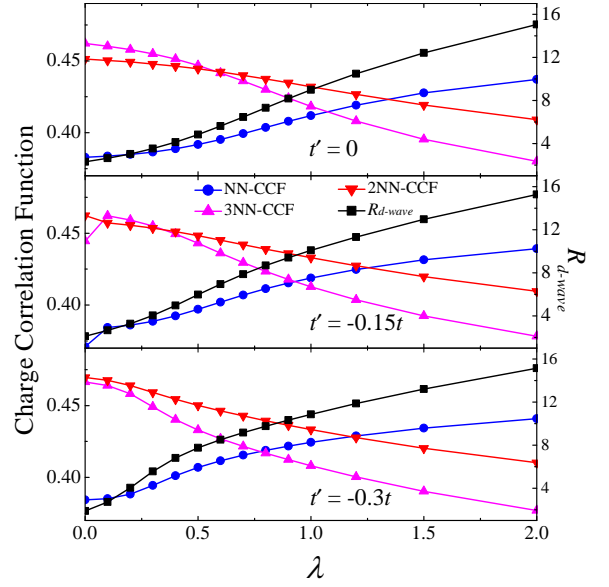


FIG. 11: The charge correlation functions (NN-CCF, 2NN-CCF and 3NN-CCF) and the ratio of the largest to second largest eigenvalue of the d -wave pair density matrix $R_{d\text{-wave}}$ as functions of d -wave pair field strength λ at 50% hole-doping. $U = 6t$ and $t'(0, -0.15t, -0.3t)$ are indicated.

d -wave SC order to a CDW state results in the formation of a checkerboard pattern as well as the reduction in $R_{d\text{-wave}}$. The transition at 50% doping (see Fig. 10) is similar to that at 37.5% doping. One interesting finding is that this QCC is dependent not on Coulomb U , but rather t' , demonstrated by the comparison between the calculations for different values of U as shown in Fig. 10 and Fig. 11. At this doping, electron density is low and double occupancy is less relevant, so Coulomb U has little effect on the properties of the ground state.

IV. SUMMARY AND CONCLUSION

Based on the above calculations at various dopings, we obtain the Hubbard model “phase diagram” tracking the λ^* as a function of doping, as shown in Fig. 12. Combined with the d -wave pair, charge and spin density matrix calculations exhibiting each order parameter, several conclusions are obtained: (i) At half-filling and in the underdoped region, the Hubbard model exhibits a strong antiferromagnetic order with λ^* depending primarily on Coulomb U . (ii) In the overdoped region, we observe a checkerboard CDW state with λ^* exclusively determined by t' . (iii) Optimal doping is achieved at 25%, where λ^* moves close to zero or even negative values, demonstrating a d -wave SC state in the pure Hubbard model. (iv) Large t' favors d -wave SC order, demonstrated in the phase diagram where λ^* is smaller at larger t' , and in the optimal doping $R_{d\text{-wave}}$ which has a larger value at $\lambda = 0$ for larger t' .

The “phase diagram” has several compelling features

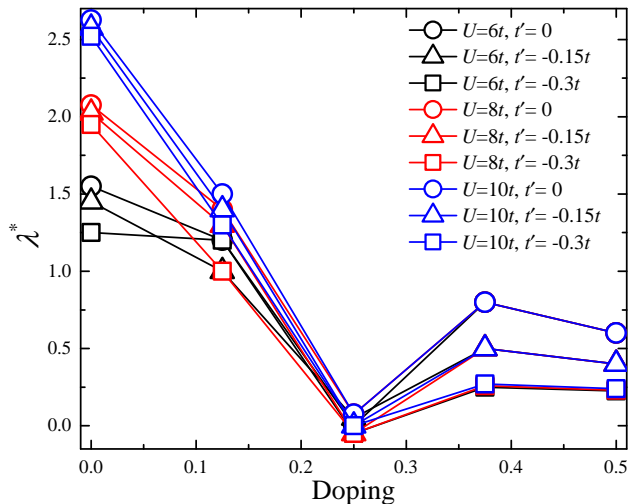


FIG. 12: Phase diagram of λ^* vs. hole-doping rate at $U = 6t, 8t, 10t$ and $t' = 0, -0.15t, -0.3t$. The 2D single-band Hubbard model favors a d -wave SC phase near 25% hole-doping, an antiferromagnetic phase at underdoped and a checkerboard CDW phase at overdoped region. Strong antiferromagnetic order near half-filling is mainly dependent on Coulomb U , while the strength of CDW far from half-filling is exclusively determined by t' .

which indicate that the Hubbard model contains rich physics which may underlie an understanding of different competing phases in the cuprates. Clearly, our results show the prevalence of antiferromagnetic order around 1/2 filling, and that t' does not assist superconductivity by suppressing antiferromagnetism. Here the dominant energy scale is the Hubbard U . At large doping a weaker checkerboard charge density wave region emerges which is controlled largely by t' . The checkerboard density-wave is more easily destabilized by the d -wave pair field than antiferromagnetism, giving smaller values of λ^* in the overdoped region. In between, it appears that superconductivity may emerge as a consequence of the battle between antiferromagnetism controlled by U and checkerboard charge density wave order controlled and suppressed by larger t' . Therefore it is tempting to intuit that the physics of t' may not be reflective of orbital content (such as apical oxygen content) or a destabiliza-

tion of the Zhang-Rice singlet, but more connected to a destabilization of a competing density-wave order. Thus it would be of great interest to explore larger cluster sizes to examine the changes of the “phase diagram” shown in Fig. 12 as a function of cluster size.

In summary, exact diagonalization techniques have been employed to study the d -wave SC phase of the 2D single-band Hubbard model. The fidelity metric g , the d -wave pair and charge/spin density matrices, including $R_{d\text{-wave}}$, R_{spin} and CCFs have been calculated for the single-band Hubbard model plus a d -wave pair field term at various hole-dopings and parameters including Coulomb U , the next-nearest-neighbor hopping t' and the d -wave SC pair field strength λ . Calculations show that at 25% hole-doping the 2D single-band Hubbard model possesses a d -wave SC ground state. Based on these results, we further summarize the behavior of λ^* as a function of doping in the phase diagram. Our phase diagram is qualitatively consistent with that from experiments⁴⁶ and dynamical cluster approximation calculations^{6,7}. Moreover, the d -wave SC order is enhanced by t' , consistent with experiments⁸ and recent multi-orbital fluctuation exchange approximation calculations⁴⁵. To obtain the d -wave SC order parameter, finite size scaling analysis could be done, provided that ED calculations on larger systems become feasible in the future.

V. ACKNOWLEDGEMENTS

CJJ, BM, CCC, and TPD would like to acknowledge L.-Q. Lee for valuable discussion and advice. This work was supported at SLAC and Stanford by the U.S. Department of Energy, Office of Basic Energy Sciences, under Contract No. DE-AC02-76SF00515 and at UCSC under Contract No. DE-FG02-06ER46319. CJJ is also supported by the Stanford Graduate Fellowships Program. A portion of the computational work was performed using the resources of the National Energy Research Scientific Computing Center (NERSC) supported by the U.S. Department of Energy, Office of Science, under Contract No. DE-AC02-05CH11231.

¹ J. Hubbard, Proc. R. Soc. London, Series A **276**, 236 (1963).

² P. W. Anderson, Science **235**, 1196 (1987).

³ F. C. Zhang and T. M. Rice, Phys. Rev. B **37**, 3759 (1988).

⁴ W. Kohn and J. M. Luttinger, Phys. Rev. Lett. **15**, 524 (1965).

⁵ S. Raghu, S. A. Kivelson, and D. J. Scalapino, Phys. Rev. B **81**, 224505 (2010).

⁶ T. A. Maier, M. Jarrell, T. Pruschke, and M. H. Hettler, Rev. Mod. Phys. **77**, 1027 (2005).

⁷ T. A. Maier, M. Jarrell, T. C. Schulthess, P. R. C. Kent, and J. B. White, Phys. Rev. Lett. **95**, 237001 (2005).

⁸ E. Pavarini, I. Dasgupta, T. Saha-Dasgupta, O. Jepsen, and O. K. Anderson, Phys. Rev. Lett. **87**, 047003 (2001).

⁹ K. Tanaka, T. Yoshida, A. Fujimori, D. H. Lu, Z.-X. Shen, X.-J. Zhou, H. Eisaki, Z. Hussain, S. Uchida, Y. Aiura, et al., Phys. Rev. B **70**, 092503 (2004).

¹⁰ J. Konior, Physica C: Superconductivity **235-240**, 2165 (1994).

¹¹ S. R. White and D. J. Scalapino, Phys. Rev. B **60**, R753

- (1999).
- ¹² T. A. Maier, M. Jarrell, T. Pruschke, and J. Keller, Phys. Rev. Lett. **85**, 1524 (2000).
 - ¹³ G. B. Martins, J. C. Xavier, L. Arrachea, and E. Dagotto, Phys. Rev. B **64**, 180513(R) (2001).
 - ¹⁴ L. Spanu, M. Lugas, F. Becca, and S. Sorella, Phys. Rev. B **77**, 024510 (2008).
 - ¹⁵ E. Khatami, A. Macridin, and M. Jarrell, Phys. Rev. B **78**, 060502(R) (2008).
 - ¹⁶ R. J. Birgeneau, C. Stock, J. M. Tranquada, and K. Yamada, J. Phys. Soc. Jpn. **75**, 111003 (2006).
 - ¹⁷ S. A. Kivelson, I. P. Bindloss, E. Fradkin, V. Oganessian, J. M. Tranquada, A. Kapitulnik, and C. Howald, Rev. Mod. Phys. **75**, 1201 (2003).
 - ¹⁸ J. E. Hoffman, E. W. Hudson, K. M. Lang, V. Madhavan, H. Eisaki, S. Uchida, and J. C. Davis, Science **295**, 466 (2002).
 - ¹⁹ C. Howald, H. Eisaki, N. Kaneko, M. Greven, and A. Kapitulnik, Phys. Rev. B **67**, 014533 (2003).
 - ²⁰ M. Vershinin¹, S. Misra¹, S. Ono, Y. Abe, Y. Ando, and A. Yazdani, Science **303**, 1995 (2004).
 - ²¹ K. McElroy, D.-H. Lee, J. E. Hoffman, K. M. Lang, J. Lee, E. W. Hudson, H. Eisaki, S. Uchida, and J. C. Davis, Phys. Rev. Lett. **94**, 197005 (2005).
 - ²² M. C. Boyer, W. D. Wise, K. Chatterjee, M. Yi, T. Kondo, T. Takeuchi, H. Ikuta, and E. W. Hudson, Nat. Phys. **3**, 802 (2007).
 - ²³ W. D. Wise, M. C. Boyer, K. Chatterjee, T. Kondo, T. Takeuchi, H. Ikuta, Y. Y. Wang, and E. W. Hudson, Nat. Phys. **4**, 696 (2008).
 - ²⁴ M. Hashimoto, R.-H. He, K. Tanaka, J.-P. Testaud, W. Meevasana, R. G. Moore, D. Lu, H. Yao, Y. Yoshida, H. Eisaki, et al., Nat. Phys. **6**, 414 (2010).
 - ²⁵ M. Rigol, B. S. Shastry, and S. Haas, Phys. Rev. B **79**, 052502 (2009).
 - ²⁶ M. Rigol, B. S. Shastry, and S. Haas, Phys. Rev. B **80**, 094529 (2009).
 - ²⁷ P. Zanardi and N. Paunkovic, Phys. Rev. E **74**, 031123 (2006).
 - ²⁸ L. Campos Venuti and P. Zanardi, Phys. Rev. Lett. **99**, 095701 (2007).
 - ²⁹ L. Campos Venuti, M. Cozzini, P. Buonsante, F. Massel, N. Bray-Ali, and P. Zanardi, Phys. Rev. B **78**, 115410 (2008).
 - ³⁰ D. F. Abasto, A. Hamma, and P. Zanardi, Phys. Rev. A **78**, 010301(R) (2008).
 - ³¹ J. Bardeen, L. N. Cooper, and J. R. Schrieffer, Phys. Rev. **108**, 1175 (1957).
 - ³² A. Steane, Rep. Prog. Phys. **61**, 117 (1998).
 - ³³ D. P. DiVincenzo and C. H. Bennett, Nature(London) **404**, 247 (2000).
 - ³⁴ P. Buonsante and A. Vezzani, Phys. Rev. Lett. **98**, 110601 (2007).
 - ³⁵ W. L. You, Y. W. Li, and S. J. Gu, Phys. Rev. E **76**, 022101 (2007).
 - ³⁶ S. Chen, L. Wang, S. J. Gu, and Y. P. Wang, Phys. Rev. E **76**, 061108 (2007).
 - ³⁷ S. Garnerone, D. Abasto, S. Haas, and P. Zanardi, Phys. Rev. A **79**, 032302 (2009).
 - ³⁸ S. J. Gu and H. Q. Lin, Euro. phys. Lett. **87**, 10003 (2009).
 - ³⁹ C. N. Yang, Rev. Mod. Phys. **34**, 694 (1962).
 - ⁴⁰ L. Gorkov, Sov. Phys. JETP **7**, 505 (1958).
 - ⁴¹ O. Penrose and L. Onsager, Phys. Rev. **104**, 576 (1956).
 - ⁴² R. B. Lehoucq, D. C. Sorensen, and C. Yang, *ARPACK Users Guide: Solution of Large-Scale Eigenvalue Problems with Implicitly Restarted Arnoldi Methods*. (Philadelphia: SIAM, 1998).
 - ⁴³ J. Oitmaa and D. D. Betts, Can. J. Phys. **56**, 897 (1978).
 - ⁴⁴ P. R. C. Kent, T. Saha-Dasgupta, O. Jepsen, O. K. Andersen, A. Macridin, T. A. Maier, M. Jarrell, and T. C. Schulthess, Phys. Rev. B **78**, 035132 (2008).
 - ⁴⁵ H. Sakakibara, H. Usui, K. Kuroki, R. Arita, and H. Aoki, Phys. Rev. Lett. **105**, 057003 (2010).
 - ⁴⁶ P. A. Lee, N. Nagaosa, and X.-G. Wen, Rev. Mod. Phys. **78**, 17 (2006).